# Measuring Pronation and Supination Using Accelerometers and Force-Sensitive Resistors

Brian Petro, Teagan Mathur, Eric Edstrom, Wilma Rishko, Jae Young Lee, Ruizhi Wang, Dominic Culotta

University of Illinois at Urbana-Champaign
PHYS 398 DLP
April 30, 2021

## Abstract

Understanding how to measure foot pronation and supination can help us understand the causes of injuries in runners and dancers. Currently, the methods of measuring these conditions are either unreliable or cannot provide concrete numerical data for deeper analysis. To create a device that is cheap and accessible for measuring levels of pronation and supination, we used an Arduino-based data logger consisting predominantly of three accelerometers and four force-sensitive resistors (FSRs). These were attached to a person's leg on their lower back calf, heel, and upper foot to measure changes in the yaw, pitch, and roll as they moved. We looked at the person standing, walking, and running in order to collect acceleration, magnetic, gyroscopic, and conductance data. We then used Python to parse and help interpret the data. Angles indicating pronation and supination were found by graphing the accelerometer data, supported by force maps of the FSR data.

# Contents

# Introduction

Foot pronation and supination, which refer to certain conditions of the foot and ankle, are common in activities such as running and dance (Willems et al., 2021). PR and SP are classified, in a general sense, as the movement of the subtalar joint, which is the articulation between the talus (ankle bone) and the calcaneum (heel bone) (Griffiths, 2021). Over angular extension of this junction has been linked to physical ailments such as plantar fasciitis, Achilles tendonitis, and back pain, as well as other issues (Willems et al., 2021).

Our study aims to better understand pronation (PR) and supination (SP) under specific conditions of dynamic motion. There has been little research done on and few methods developed for studying PR and SP under dynamic motion, such as walking and jogging.

# Background

PR and SP can be qualitatively described by looking at qualities such as the foot's arch, a person's shoe wear pattern, and surface area contact shape with a flat surface (Erickson et al., 2009). To quantify PR and SP, angular ranges are measured of how the ankle joint moves with respect to a reference. Figure 2.2 shows two of these angles on a right leg. The reference is the perpendicular line that runs up from the ground through the middle of the Achilles tendon, just above the heel. In a normal, neutral stance the line goes through all the red points. The angular displacement that the calf and lower heel points make from the reference line are two of the angles of PR and SP that we are interested in recording for this experiment.

This method of measuring PR and SP is based on a paper by Genova and Gross (2000), but slightly modified. The main difference is that Genova and Gross use the midline of the calf as a reference line, and measure the angle that midline of the heel makes with it when the two intersect. An example of Genova and Gross's unmodified method appears in Figure 2.1.

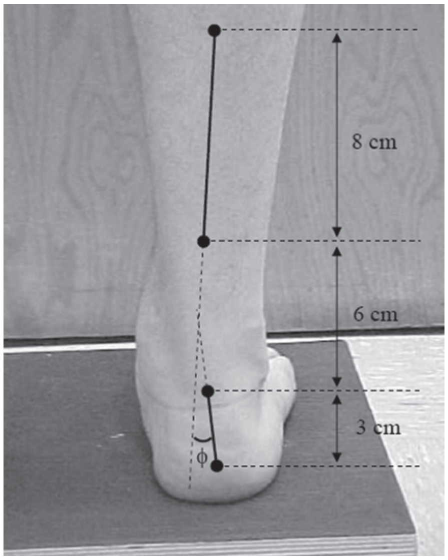

Figure 2.1: The method of measuring pronation used by Genova and Gross (Tsai et al., 2006)

This method creates only one angle to measure, while we have two with our method. Genova and Gross's angle would be equal to the difference of our two angles. The top angle is subtracted because it is the reference for the lower angle. Our reference line splits Genova and Gross's angle into two angles. The angle on the calf that we are measuring is the opposite vertical angle of the leftover angle to the left of our reference that was created when splitting Genova and Gross's angle. This deviation was made to make the measurement more easily obtainable using accelerometers. As mentioned before, some PR and SP is normal; so, to distinguish between overpronation and supination, we used cutoff angles from Genova and Gross. The cutoff values correspond to the difference of the two angles, not each one individually. For pronation, the cutoff angle would be a resultant angle greater than 10°. For supination, the cut off angle would be a resultant angle less than 3°.

Another angle that we tried to measure was the angle by the foot rotating around a line parallel to the length of the foot. The angle could be captured by defining a point in the top of the foot. This method would be used as a general reference to the our more rigours method described in the above paragraph. If the foot moves inward then it would be pronation. If it moves outward then it would be supination. Figure 2.1 shows how we placed accelerometer 0 on the subject's shoe laces to capture this angle.

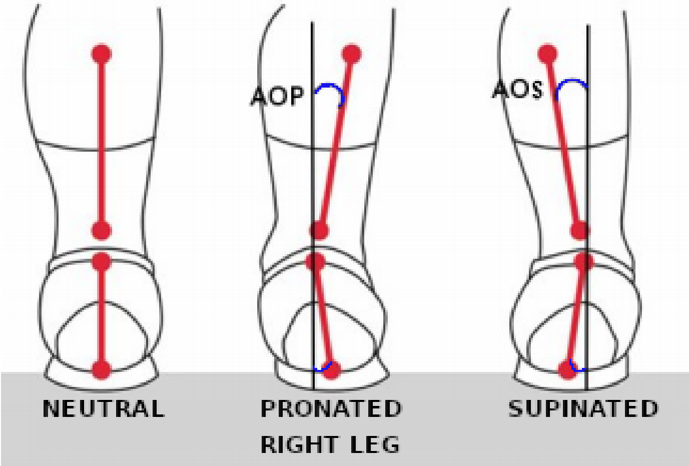

Figure 2.2: Pronation and supination classified in humans. Angle of pronation is denoted by AOP, and angle of supination by AOS (Erickson et al., 2009)

The second way that PR and SP is quantitatively measured is to measure how pressure is distributed on the bottom of the foot. In a study where they examined associations between foot posture and foot function, and foot pain, PR and SP were measured using a pressure mat on which subjects would stand (Menz et al., 2013). Their results were heat maps that show how a person distributed their weight on the pads of their feet while bearing additional weight. Figure 2.3 shows a sample of their pressure maps where red shows the areas of highest pressure and blue the areas of lowest pressure. This figure is also of a subject whom they considered to be neutral, not severely pronated or supinated. In this experiment, we would expect to find subjects who pronated to have more pressure toward the under arch and less on the outer edges of the foot. For supination, we would expect to find more pressure on the outer edges, and very little or no pressure under the arch.

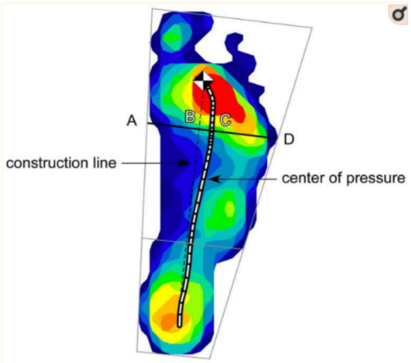

Figure 2.3: Center of pressure calculation from dynamic foot pressure map (Menz et al., 2013)

Based on these static measurements, individuals are often prescribed a shoe intended to correct their stride (Neumann, 2017). However, recent studies have cast doubt on the reliability of this method (Richards et al., 2009). Indeed, Neumann concludes that “no validated algorithm yet exists to determine the appropriate shoe for an individual that will minimize injury risk while maintaining or improving performance” (p. 719). Given the uncertainty over how best to assess an individual’s needs for a particular shoe, and the apparent unreliability of measuring static foot posture, we decided to try developing an alternative method of measuring PR and SP in runners and others. Our primary goal was to measure foot posture during the act of running itself, seeing as this is the activity during which injury risk is maximized. This, we hoped, would provide a more realistic measure of a person’s tendency to pronate when running, and may better inform the decision of what type of shoe they should wear.

Measuring the foot pronation or supination of a runner in motion is no trivial task. To obtain accurate data, we would need to account for a number of factors. First, we would need to design a reliable and quantitative method for measuring pronation while running. Second, we would need a way to easily manipulate the data, in order to correct errors, analyze the data in different ways, and elegantly present it to others. Finally, we would need our method to be repeatable by others, so it would need to use readily available components with easy assembly. With these considerations in mind, we set out to design our data acquisition unit.

# Methods

## 3.1 Overview

We used an Arduino Mega 2560 along with three Adafruit LSM9DS1 units and four force-sensitive resistors to create our data logger for the data collection. The LSM9DS1s each contain an accelerometer, a gyroscope, and a magnetometer, which were used to measure the AOP and AOS. The force-sensitive resistors enabled us to measure the force from regions of the subject's foot. These instruments communicated using the I2C protocol and were physically attached to the subject's leg using elastic bandages. We then analyzed the data using Python code to determine a subject's level of pronation or supination. Using this method, we were able to accurately and repeatably measure the strides of various subjects. An explanation of these various components follows.

### 3.1.1 List of Devices

The following is a detailed list of the devices that we used to communicate with the Arduino: a 4x3 keypad, a Real-Time Clock unit (RTC), an Adafruit Ultimate GPS Breakout v3, a 16x2 Liquid Crystal Display (LCD), a microSD breakout board, three LSM9DS1s, four force-sensitive resistors (FSRs), and an I2C multiplexer. The Arduino used a battery pack and 5V power supply to run the devices.

### 3.1.2 Arduino and I2C

The Arduino Mega2560 board combines the Atmel ATmega2560 microcontroller with a variety of ports and interconnect options. It uses a modified version of the C++ language to run user-defined programs. In this way, a nearly limitless number of use cases are possible. For our project, we decided to use the I2C protocol to connect our devices together.

I2C, or Inter-Integrated Circuit, is a simple digital communication protocol using two wires for each connection which emphasizes ease-of-use over raw performance. I2C uses the boss and staff model.

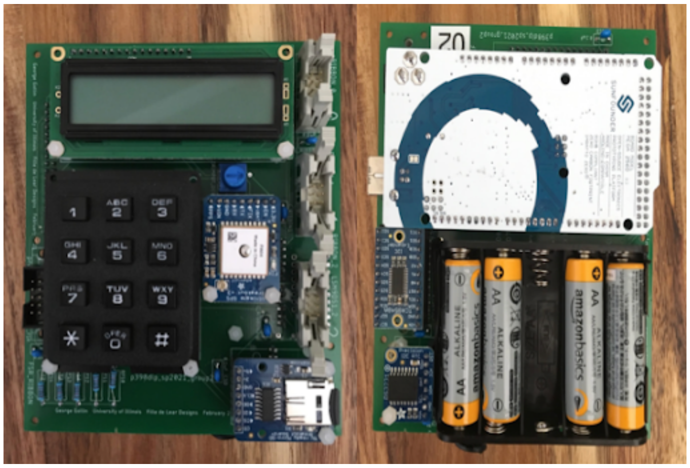

Figure 3.1: Arduino data acquisition device

*Boss* refers to the microcontroller in the main Arduino board that sends commands and instructions to the peripheral devices, which are referred to as *staff*. A competing protocol to I2C, Serial Peripheral Interface, or SPI, has a four wire communication system and is faster than I2C. However, SPI only allows for one boss capability, whereas I2C has multiple boss capabilities. Data in SPI can be shared between the boss and staff in two ways—it is full duplex. Two frequencies are used to transmit and receive information. I2C, on the contrary, is half duplex, meaning data can flow in both directions, but not simultaneously. I2C was chosen in our case because it allows for multiple peripheral devices to be connected at one time with minimal wiring while still maintaining a fast enough read speed for each device.

One disadvantage of I2C is that it assigns a unique identifier to each device model, meaning it cannot distinguish between multiple of the same device. To overcome this, we made use of an I2C multiplexer, a device which takes two or more of the same device and assigns them distinct identifiers before connecting them to the boss.

### 3.1.3 GPS and RTC

The GPS receives data from up to 22 satellites and provides data on location, speed, date, and time. The Real-Time Clock (RTC) was synchronized with the GPS in our data logger to create accurate timing for our data set. It was also used to get the date and time of when the data were collected for easy synchronization with video data taken from a separate device.

### 3.1.4 Timing and Data Logging

An SD card was used to store the accelerometer data, the elapsed time obtained from the Arduino `millis` function, and the real time and date from the RTC. The `millis` function gives the number of milliseconds passed since the Arduino program started running, it is a useful and accurate way to sync up the data collected from the different sensors to the time passed since the start of the program. To monitor the data collection and aid in offline analysis, an LED was installed on each accelerometer and set to blink once at the beginning to signal the start of the program, and continue blinking once every half second thereafter. This acted as a visual marker to synchronize the data with a video that was being taken of the runner.

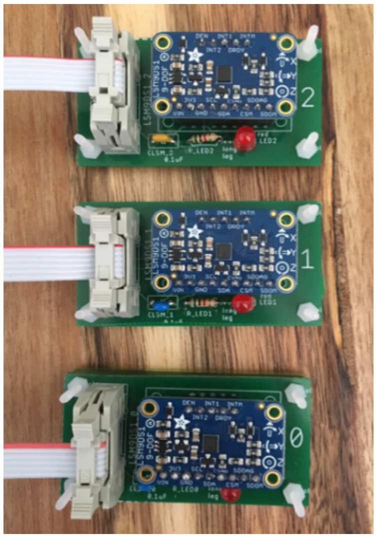

Figure 3.2: The three accelerometers and their respective LEDs

### 3.1.5 Python

For post processing, Python was chosen as the language to handle the offline analysis of these data. Python is an interpreted language written by Guido van Rossum. Part of the philosophy behind Python's creation was that "simple is better than complex" (Peters, 1999, as cited in Python Software Foundation, 2004, p. 1). Following this mantra, Python has straightforward syntax which makes developing programs much faster than developing those same programs using other languages. This simplicity often results in programs that take longer to run than in other languages; however, given the nature of offline analysis, this trade-off did not present any issues to this project. The reduction in time to write code vastly exceeded the time that would have been saved by writing the same code in another language. In addition to simple syntax, Python has a rich and easy-to-use collection of third-party libraries for data analysis.

## 3.2 Making and Using the Parts

The thought process behind the design was to find a way to create a system that would be sensitive enough to changes in an angle but also maintain a degree of rigidity when in a jogging motion. The part that we first focused on was deciding on the orientation of the accelerometers on a person. Figure 2.2 shows the AOP and AOS that we are interested in; we decided to place accelerometers on the upper and lower red lines. These AOP and AOP changes correspond to rotations around the accelerometers' $x$, $y$ and $z$-axes, known as roll, pitch, and yaw. Roll, pitch, and yaw are further explained later in this section. For the orientation of the accelerometers seen in Figure 3.3, the roll angle of accelerometers 1 and 2 correspond to the AOP or AOS as seen in Figure 2.2. For accelerometer 0, the pitch corresponds to the AOP or AOS.

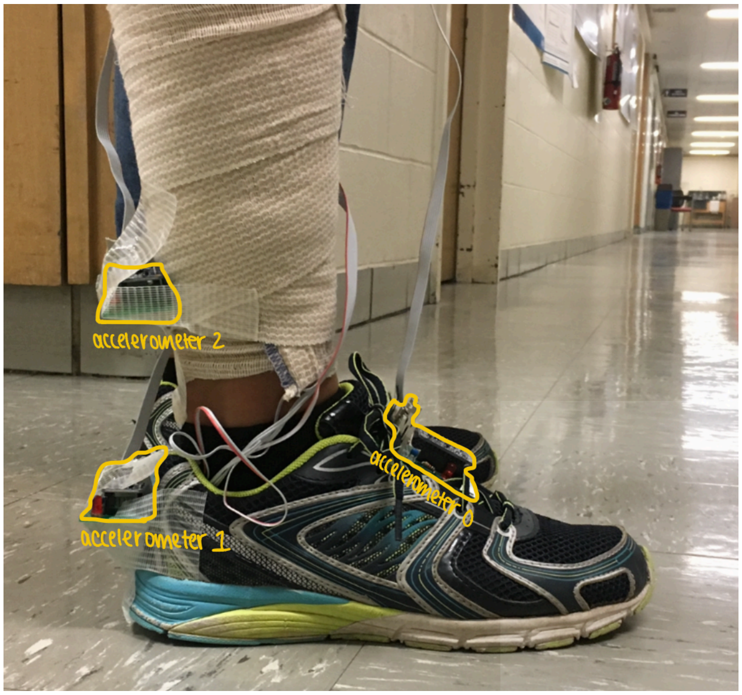

Figure 3.3: Accelerometer placement on foot and calf

Each accelerometer had a hard plastic back that was 3D printed to secure our individual accelerometers. These were mainly for the comfort of the runner, but they also served as protection against possible short circuits that might occur on the back of the printed boards' exposed solder joints.

The three LSM9DS1 breakout boards can collect gyroscopic and magnetic field data, in addition to acceleration data. When we speak of gyroscopic data, we refer to the measurement of angular velocity when rotated around self-defined axes. Accelerometers cannot directly measure angular displacement, it must be derived. This explained later in the paper under the section **Making and Using the Parts**. The accelerometer sensor has measurement ranges of ±2 $g$, ±4 $g$, ±8 $g$, and ±16 $g$; we used ±4 $g$. On Earth, $g$ is equal to 9.8 $\frac{\mathrm{m}}{\mathrm{s}^2}$. The magnetometer a range of ±12 G (Gauss), which refers to the magnetic flux density. The gyroscope a range of ±2000 deg/s. We were able to collect data at up to a rate of 83 Hz for the three devices, or about once every 12 ms (Adafruit Industries, 2021).

Figure 3.4: Computer-aided design file for the strong accelerometer back

## 3.2.1 Nautical Angles

Each accelerometer has its own predefined right-handed $x$, $y$, and $z$ coordinate system relative to itself. The rotational displacement around these axes are referred to as roll, pitch, and yaw. They are commonly referred to as *nautical angles* or *airplane angles*, as they are used in sailing and aeronautics to describe rotation around a system's axes. The following is how roll, pitch, and yaw are related to the axes.

A positive roll is a counter-clockwise rotation around the $x$-axis. A positive pitch is a counter-clockwise rotation around the $y$-axis. A positive yaw is a counter-clockwise rotation around the $z$-axis. Figure 3.5 illustrates these rotations as we defined them. Figure 3.6 on the next page shows how the coordinate systems of each accelerometer would be oriented in test setups.

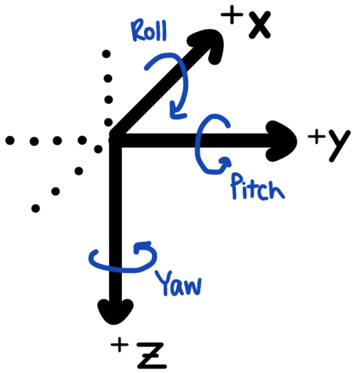

Figure 3.5: Nautical angles

## 3.2.2 How Roll and Pitch are Calculated

As mentioned previously, the accelerometers can only measure an angular velocity. For an angular displacement to be extracted from from the angular velocity, each angular velocity datum would have to be multiplied by the delta time between each sensor reading. These resulting angles would then be added to

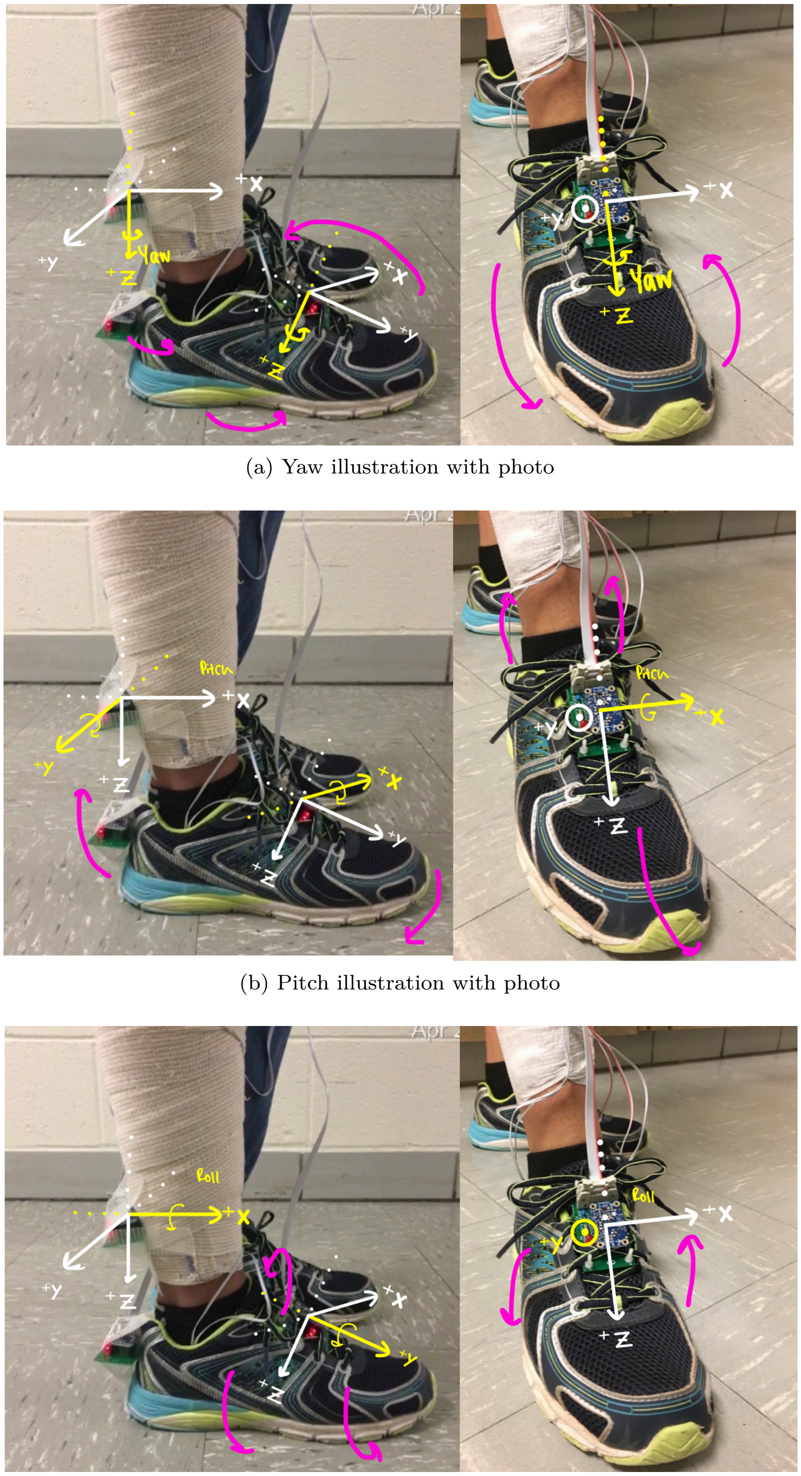

(a) Yaw illustration with photo

(b) Pitch illustration with photo

(c) Roll illustration with photo

Figure 3.6: Illustration of nautical angles with photos

each other sequentially so at any time the sensor would know how much it has tilted. This method is also known as integration. While this is the most straightforward method of calculating roll and pitch, it can rarely be used because gyroscopes are prone to drifting and overshoot. As more and more overshot data are added to the roll and pitch, the readings become less accurate.

To alleviate this, another way to calculate roll and pitch is to use the force of gravity that the accelerometers can detect at all times. This is done by calculating the angle that is created between the coordinate system of the accelerometer and Earth's coordinate system. Earth's downward direction, $z$, is determined by the direction of gravity. This is what each accelerometer then compares to its $x$ and $y$-axes to calculate roll and pitch. The idea behind this is visually represented in Figure 3.7 As a disclaimer, the labels and orientation of the block in Figure 3.7 do not represent coordinate systems and angles exactly.

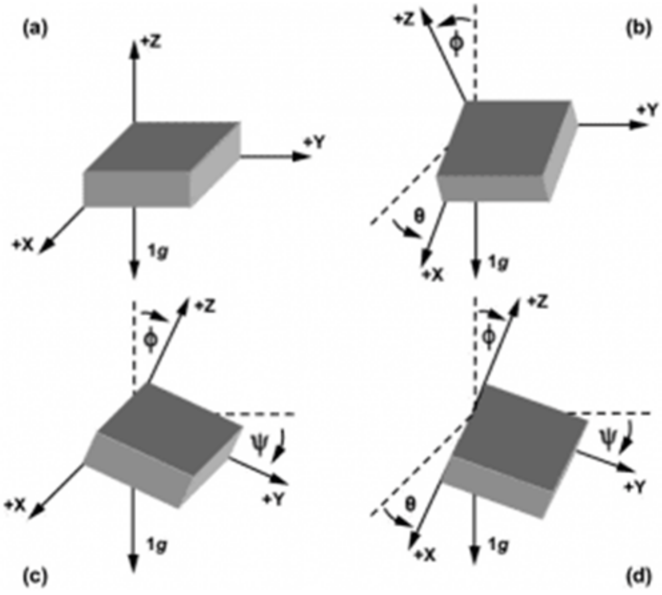

Figure 3.7: Angular displacement between Earth's and the accelerometers' coordinate systems (Newton, 2020)

The following equations for roll and pitch were used in the offline analysis:

$$\text{roll} = \arctan\left(\frac{a_y}{a_z}\right) \tag{3.1}$$

$$\text{pitch} = \arctan\left(\frac{-a_x}{\sqrt{a_y^2 + a_z^2}}\right) \tag{3.2}$$

The $a_x$, $a_y$, and $a_z$ is how the gravitational field vector is separated into components based on the orientation of the accelerometer's coordinate systems relative to it. A derivation of 3.1 and 3.2 is beyond the scope of this paper; for a full treatment, see Pedley, 2013. Yaw was not used in this study because it is the least accurate method to calculate angular displacement. It cannot solely use gravity because the gravitational vector points along the $z$-axis of the accelerometer. When both coordinate systems are aligned, rotating around it provides no change to a reference axis. The best option would be to use Earth's magnetic field as a compass and make magnetic north the reference axis. This would be done with the magnetometer that comes on board the LSM9DS1. While this works, magnetometers tend to read more slowly and unpredictably than accelerometers, so their readings will be inherently less accurate than those of the other sensors.

### 3.2.3 The Complementary Filter

While the previous method generally yields more consistent results than solely integrating, it can only be used accurately in static and slow moving cases. This is because if the sensors detect other accelerations that are not from gravity, then those will distort the direction of the gravitational vector to the sensor, which leads to inaccurate readings. The solution was to combine both methods. This is what is called a complementary filter, where the angle from integrating acts as a check to the angle being calculated from using Earth's gravity. The following equation, taken from Grahn, 2017, is the implementation of the complementary filter:

$$\text{angle}_{\text{complementary}} = \beta \cdot \text{angle}_{\text{integrate}} + (1 - \beta) \cdot \text{angle}_{\text{gravity}} \tag{3.3}$$

$\beta$ is known as the filter coefficient. This parameter determines the percent usage of each of the calculation methods. First, a percent value of the angle by gravity is taken; then, the remaining percentage is taken from the angle by integration. These two percentages are then added together to get the final, more accurate value. In our calculations $\beta$ was set to 0.93, or 93%, because we wanted to use more of the angle from gravity than from integration, as it is more accurate. The percentage from integration would consequently be 0.07, or 7%.

### 3.2.4 The Kalman Filter

An even more advanced method utilizes the so-called Kalman filter. This filter uses Bayesian statistics to better correct for error. It works in a two-step process. First the filter predicts the current state variables and their uncertainties using the previous measurement, then, once the current measurement is taken, it updates its estimates using a weighted average. In this way, the filter creates better and better estimates as it is run. The traditional Kalman filter assumes the system is linear;

however, nonlinear extensions have been developed.

The great difficulty in using the Kalman filter is in its setup. For multi-dimensional systems, such as ours, its use requires the development of several matrices to calculate the state of the system. Additionally, the algorithm itself is quite tricky to implement. While several esoteric libraries exist to facilitate its use in Python, not all of them are well-documented, and the ones that are are not necessarily straightforward to use. Ultimately, we determined that the investment of time required would not be worth it, when the complementary filter gave us good results by itself.

### 3.2.5 Force-Sensitive Resistors

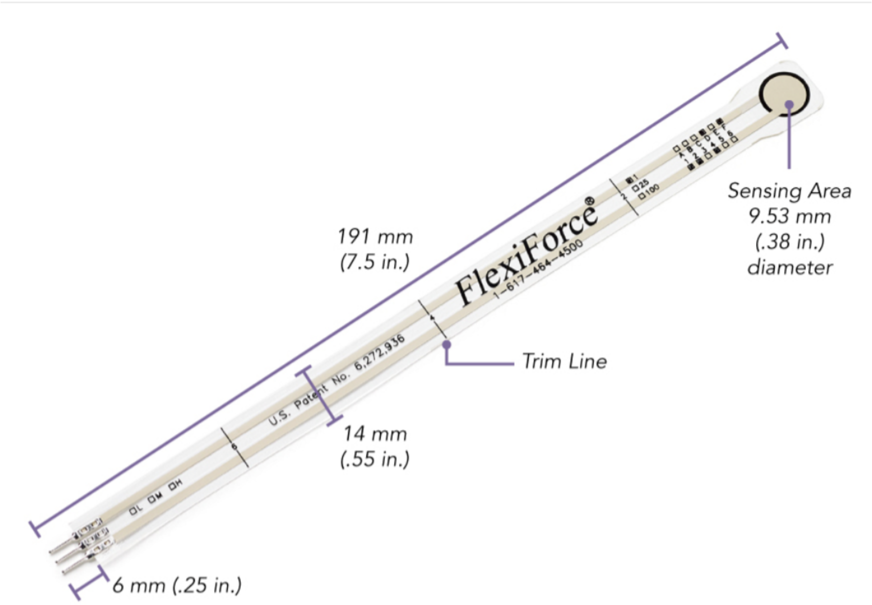

Figure 3.8: The FlexiForce A201 force-sensitive resistors used in our study with max 100 lb sensing (Tekscan, 2021c)

After placing the accelerometers, we chose the placement of the FSRs on the pads of the feet. Their placement was straightforward as we followed the method outlined in Menz et al. (2013) (see Figure 2.3 from their work). The placement of the FSRs was also chosen after some subject testing in different shoes. A foam insert of the running shoe was used to attach the FSRs as shown in Figure 3.9.

The use of only accelerometers to detect PR or SP would be difficult due to factors such as noise and synchronization of the data to the runners gate. The inclusion of FSRs allowed for better conclusions to be drawn and helped connect the data that were being collected from the accelerometers to the phases of a runner's gate as seen in Figure 3.10. For example, an FSR on the heel would likely get the most force during the heel strike phase. The FSRs are circular pads which record a change in capacitance when

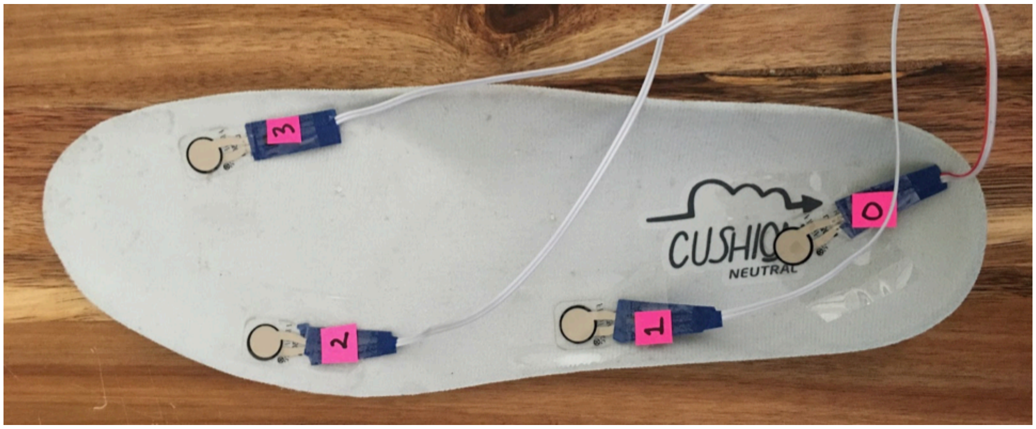

Figure 3.9: Force-sensitive resistor placement on sole of shoe

depressed. This change in capacitance can then be converted to a force. Each FSR has range from 0 to 100 lbs.

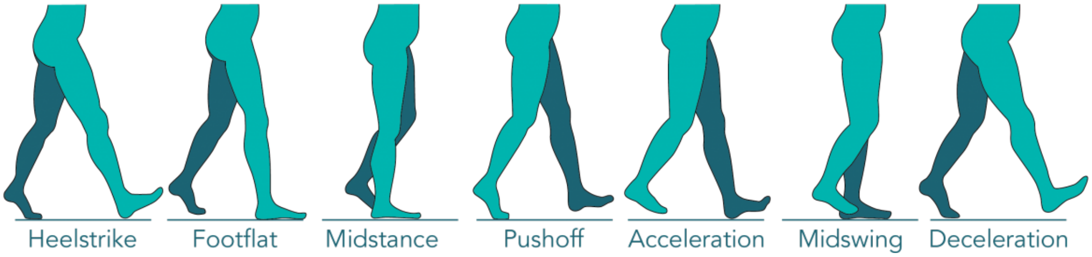

Figure 3.10: Phases of the human gait cycle (Tekscan, 2021a)

The way the raw analog to digital conversion (ADC) values were converted to pounds of force was by performing the following calculations and calibration in post processing. If we know the maximum ADC value, the ADC reference voltage, and the series resistance in the circuit, we can calculate the conductance of the FSR, $G_{FSR}$.

$$V = \frac{V_{ADC}^{ref} \cdot ADC_{count}}{ADC_{max\,count} + 1} \qquad R_{FSR} = \frac{V_{ADC}^{ref}}{V - 1} \cdot R_{series} \qquad G_{FSR} = \frac{1}{FSR} \tag{3.4}$$

Since the relationship between the conductance and force is linear, all we had to do was perform some calibration tests and experimentally find the force for each sensor. This is also why we chose to use force conductance and not resistance. We placed multiple objects of known weight on the FSRs and recorded the weight and conductance after converting the ADC count. Each object was weighed multiple times and for an extended period of time to get the most accurate data. A linear fit was created for the data and the line model was the relation between the conductance and the force.

Around 40 data were taken for each of the four masses corresponding to 0.18 lbs, 0.7375 lbs,

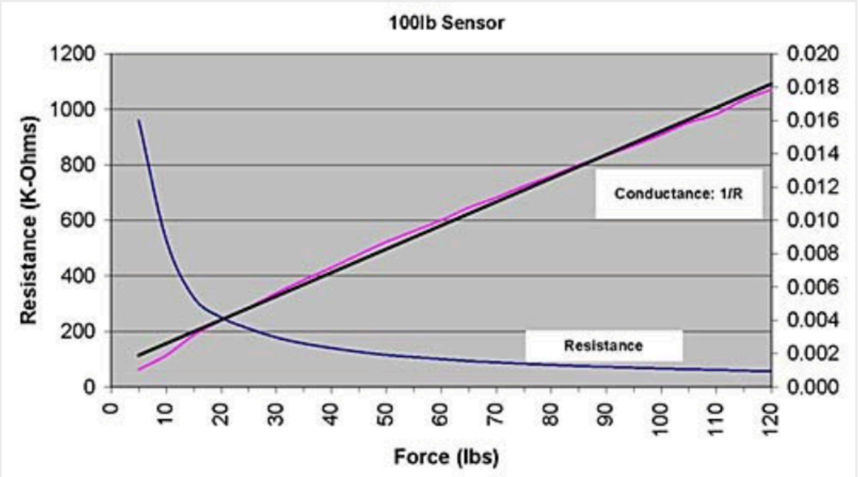

Figure 3.11: Graph of conductance vs. force (Tekscan, 2021b)

1.4125 lbs, and 2 lbs. You can see in Figure 3.12 for the middle 2 masses, we only saw 2 differing conductance values read from the FSRs. The known mass object that we used for the 2lb mass was a water bottle. We had to balance this unstable and oddly weighted mass on a small funnel so that the mass would be concentrated on the 0.38 inch diameter FSR. This is most likely why six different conductance values were measured for the 2 lb mass. A line of best fit was then used to determine the relationship between conductance and force.

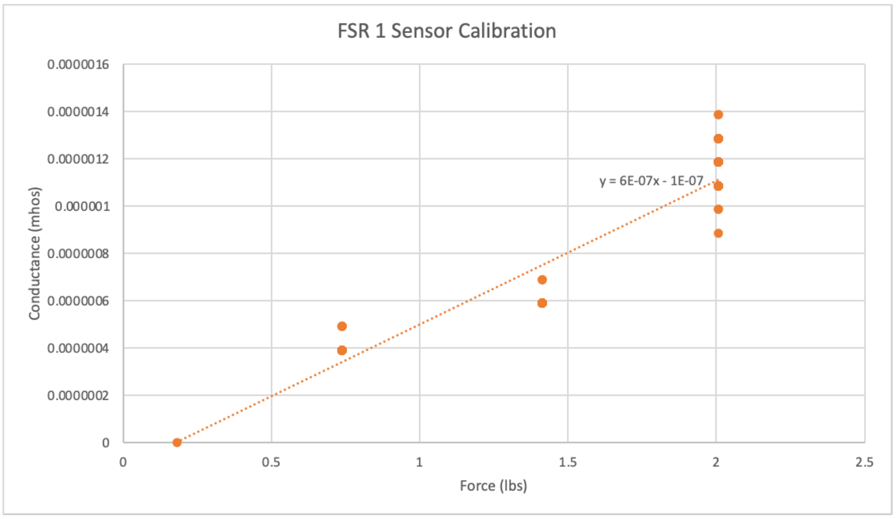

Figure 3.12: Line of best fit for experimental data relationship between conductance and force in pounds

We can see in Figure 3.12 that the equation found relating conductance in mhos, $G$, to force in pounds, $F$, is $G = 6 \times 10^7 \cdot F - 10^{-7}$. This equation can be reorganized to solve for force since that is how we will be using it.

$$F = \frac{5}{3}G + \frac{1}{6} \tag{3.5}$$

For data analysis, we used the Matplotlib, NumPy, and Pandas Python libraries. They allowed for data loading, cleaning, and visualization in only a few lines of code. Graphs were created for the nautical angles with respect to time to find trends and patterns in someone's stride, and compared with resting data to look for PR and SR. A force-map of the FSR data was created to visually show the distribution of forces during a trial. To gauge the reliability of the sensors, we found the average angles and accelerations from a resting frame using simple calculations.

Now with all the data sensors in place, they needed to be connected to a data acquisition device (DAC) to mainly read and record the data to a digital file to be read later by processing software in Python.

## 3.3 DAC Casing

The design of the DAC had a movable lid so we could insert and draw the lid through the grooves on each side of the case. We also made openings on the lid to make the number pad, LCD, and ribbon cable connections visible, which made the setup of the devices easier and enabled monitoring of the system when collecting data. There was an opening on the bottom of the case below the battery pack to enable quick removal and reinstallation of the batteries so the system could be reset between trials.

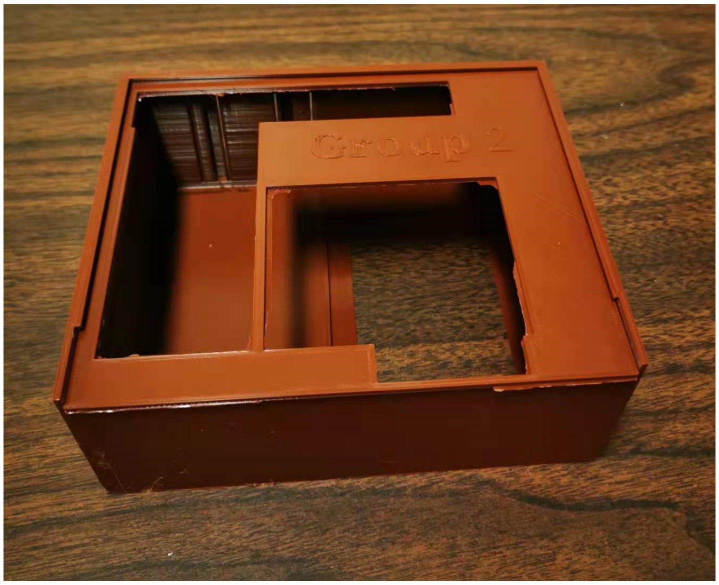

Figure 3.13: 3D-printed case for the data logger

## 3.4 Field Tests

Once the data acquisition program was loaded into the PCB, the LCD displayed a message to help verify that the SD card was working properly. The LED lights then blinked for three seconds to indicate the setup was complete and the program was ready to collect data. Additionally, an LCD display was programmed to display any error messages when the other devices were initializing.

To start data collection, the person being tested pressed the star key (*) on the keypad, and then the data logger started collecting the accelerometer and FSR data. Once the person has completed running or walking, they will press the pound key (#) to stop data collection. Doing this allowed for multiple trials to be taken without extra unneeded data being taken in between trials.

Supplemental video was taken to correlate what the data were showing when graphed to what was happening in the real world. Video recording was performed by having another person follow alongside the runner while the camera was on a rolling cart. The video, along with the time the DAC program started taking data, was timestamped to synchronize the time scales of the data and the video.

Three types of field tests were performed. The first test had the subject standing still in a neutral position to acquire data on pronation and supination in a static case. This would also allow for comparison with dynamic cases that followed, providing a baseline against which to compare the data. The second test had the subject walking, and the third lightly jogging. The goal of the different tests was to have a variety of data, and to see if pronation or supination would be more obvious in a dynamic or a static case.

Since we did not have subjects who had a known medical history of PR or SP in their limbs, we chose to have one of our subjects emulate PR and SP to the best of their ability and then do the three tests again. These tests will be referred to as their number first, then PR or SP.

# Results

Data were collected from three varying tests from two subjects. Displayed below are data of the angular displacement and force graphs taken for Subject 1 in a neutral standing stance. The initial values differ because the filter is calibrating the data.

The vertical violet lines represent when the subject's heel strikes the ground. In other words, when a new step is taken. However, because these are stationary data, this line represents a slight shift of the subject's body weight. That is why the plot's values vary on either side of that line.

The next data were of the subjects walking at a slow, controlled pace.

The steps were isolated using the FSR data to solidify patterns in the data. A step begins when the heel (0) hits the ground.

The data collection rate for the FSRs is limited by the data collection rate of the LSM9DS1 accelerometers. Unfortunately, the rate at which they were taking data was slower than for other datasets; however, it is fast enough to be accurate in distinguishing between steps. Figure 3.9 maps the numeric labels of each FSR to its location in the subject's shoe.

The third trial was of each of the subjects jogging at light pace on a flat, indoor surface.

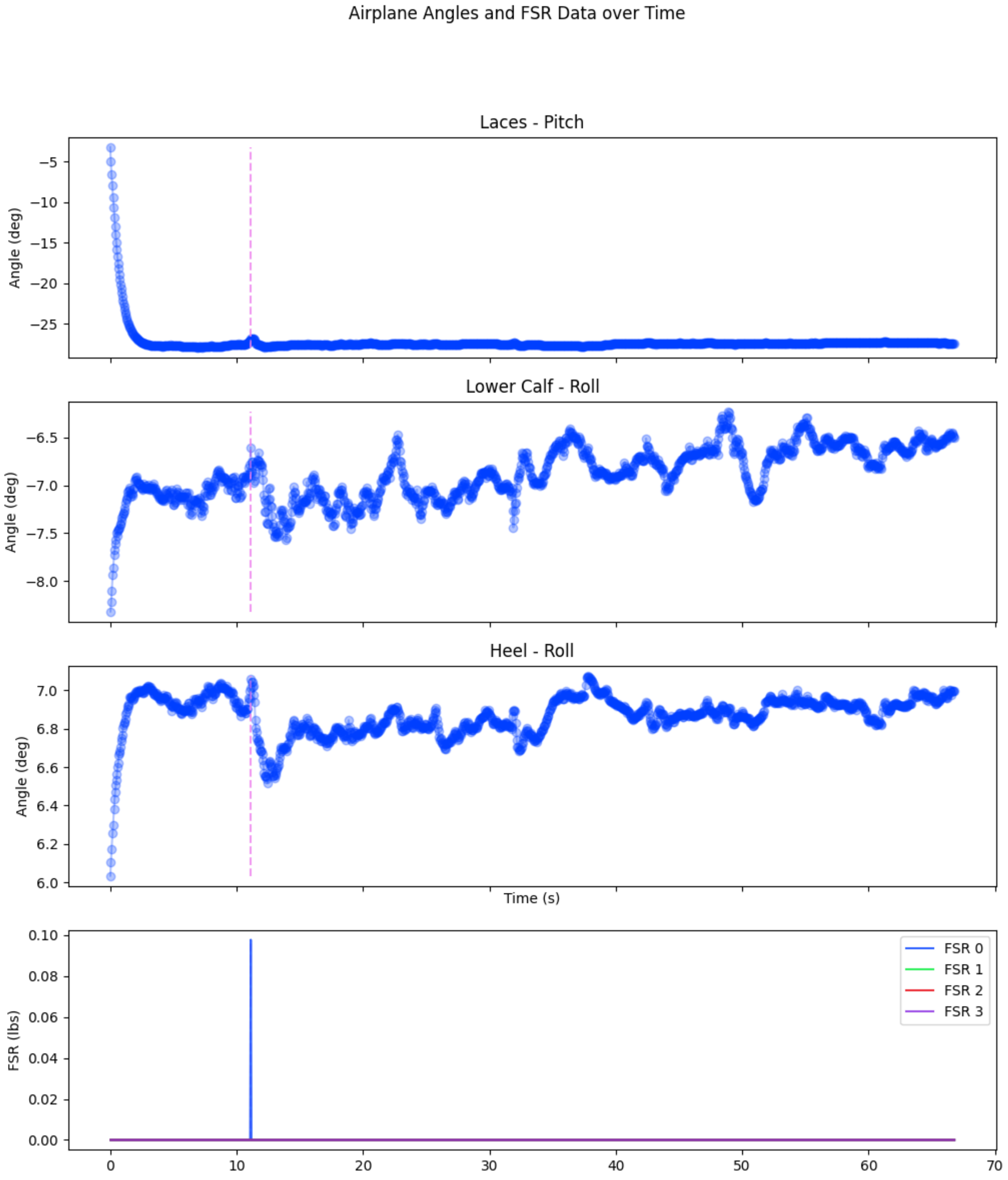

Figure 4.1: Stationary stance data

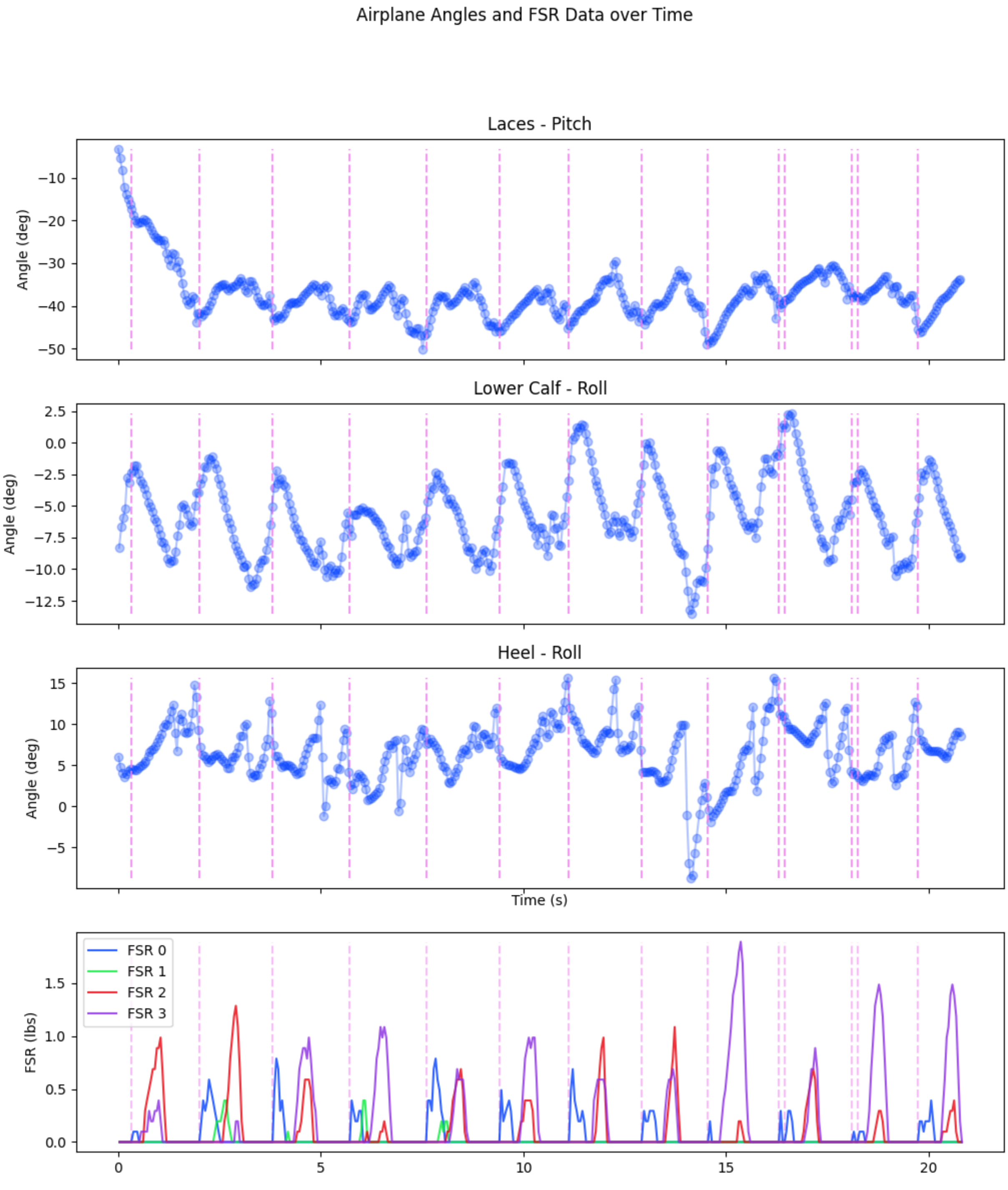

Figure 4.2: Slow controlled walking data

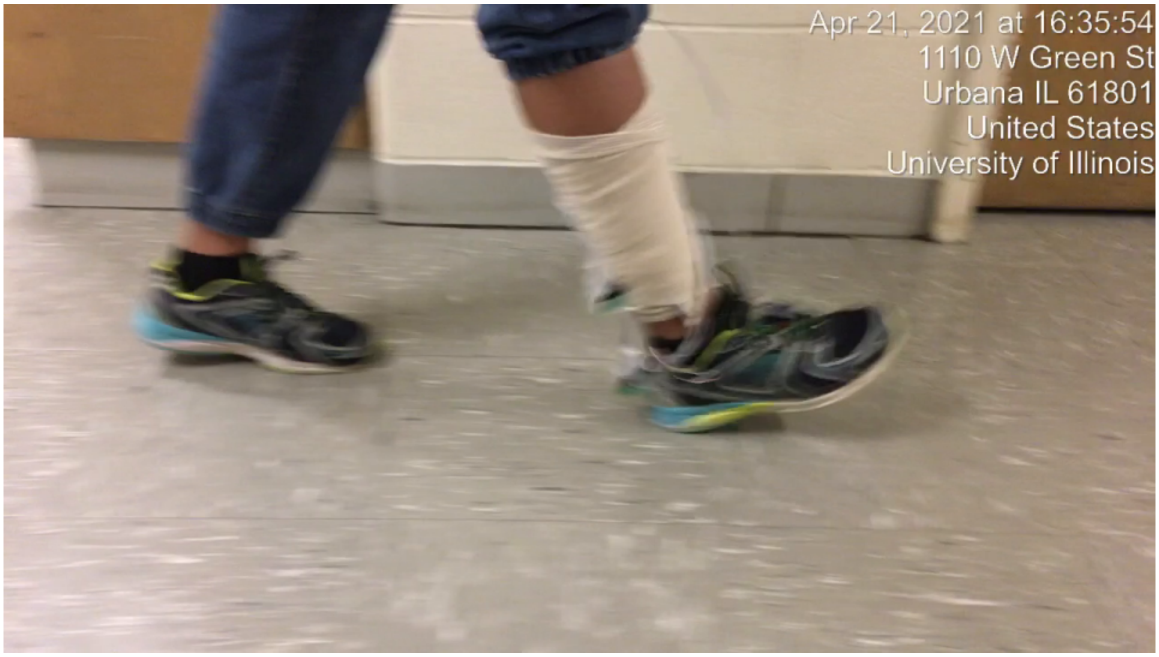

Figure 4.3: Video frame of slow controlled walking

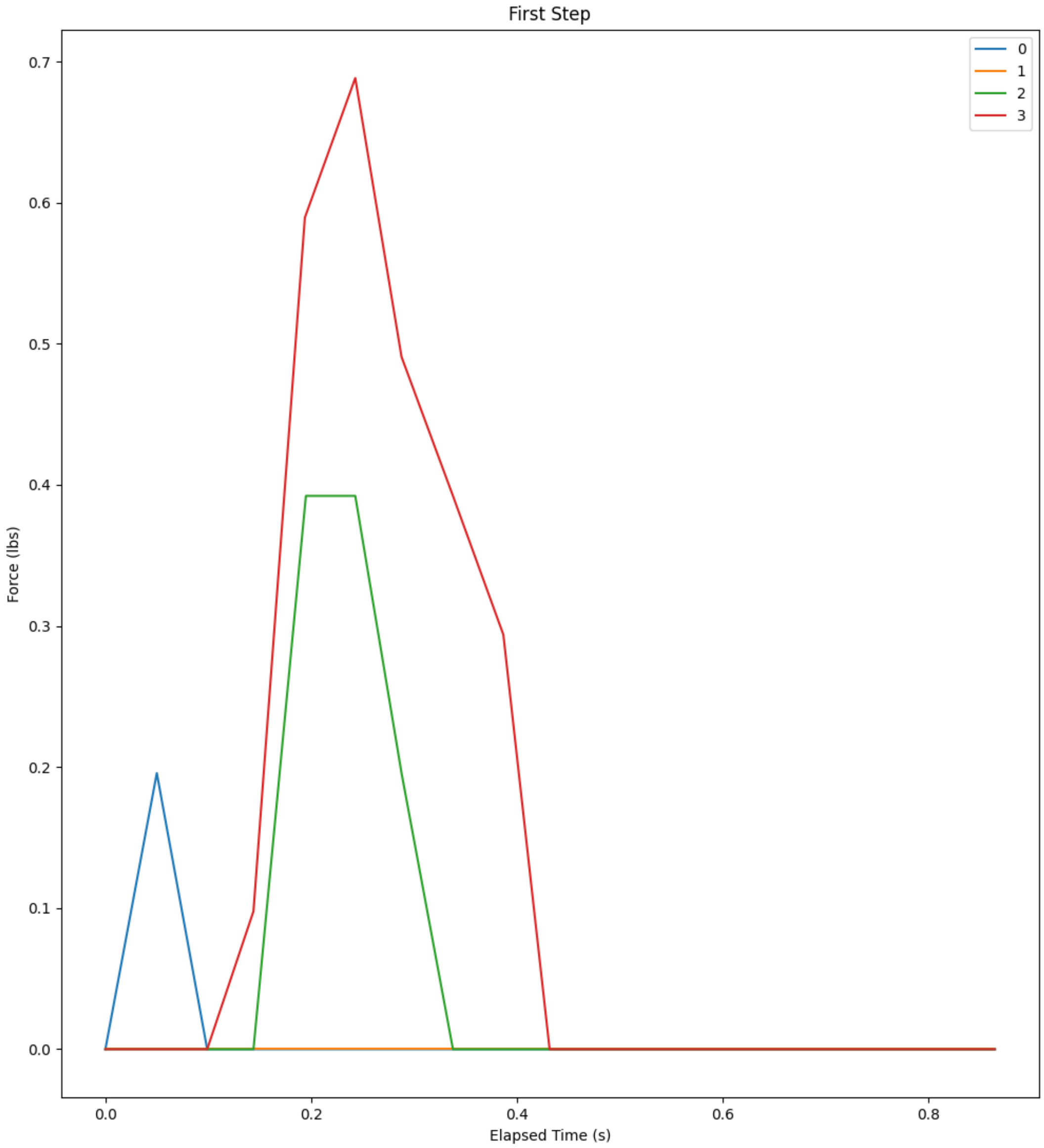

Figure 4.4: FSR values for an individual step in the walk

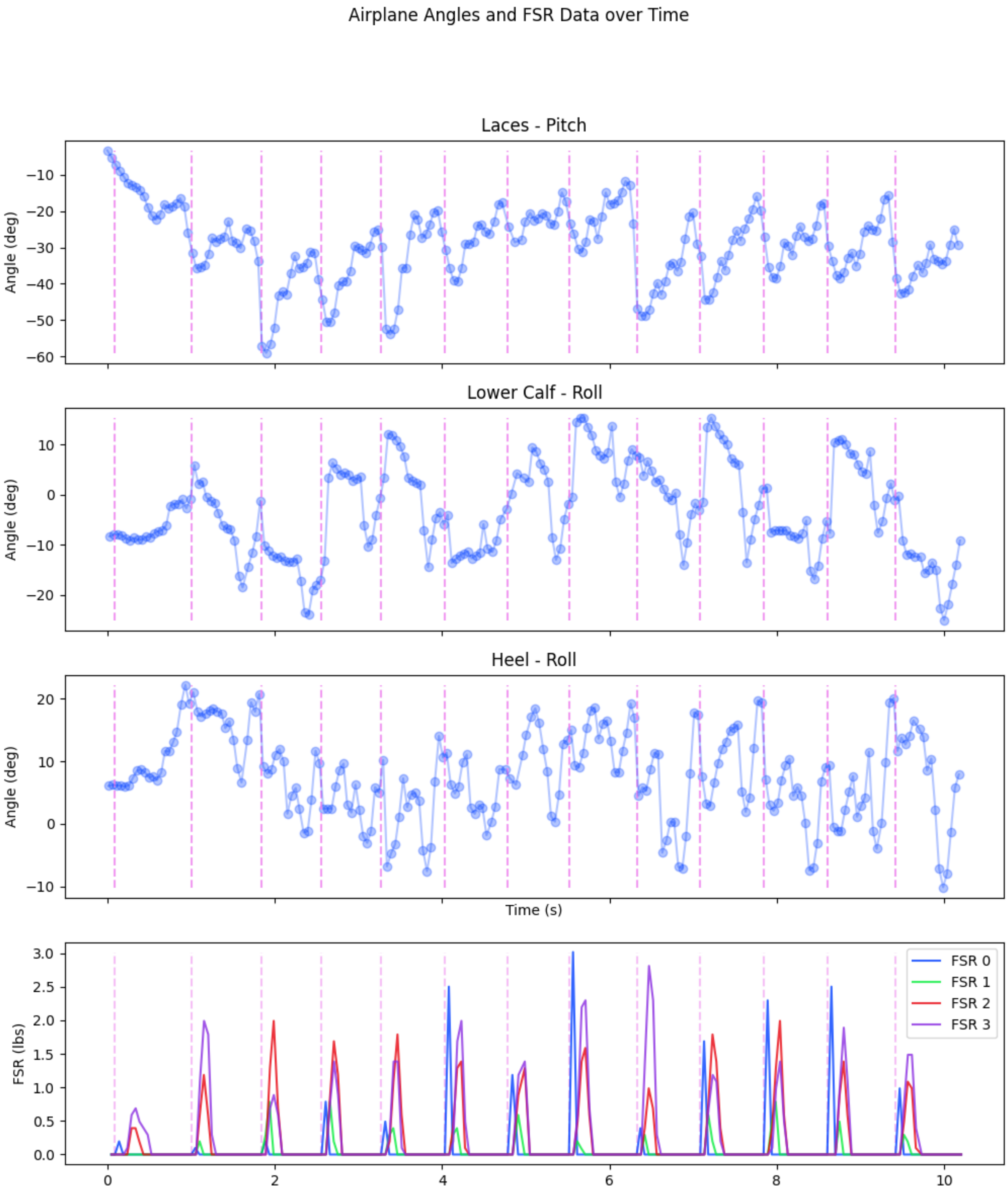

Figure 4.5: Brisk jogging data

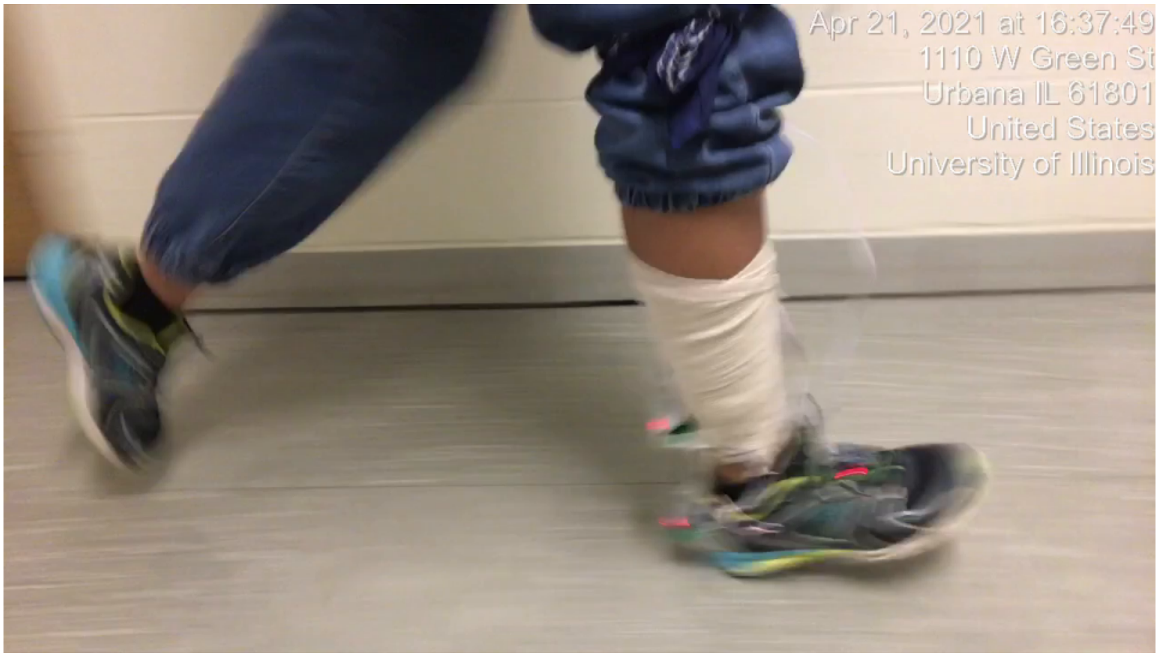

Figure 4.6: Video frame of brisk jogging contact point

# Discussion

Beginning with the standing data graphs, data were collected to develop a strong base line for each subject's neutral standing posture. Subject 1's standing data show that the accelerometer on the lower calf is recording, on average, a $-6.8°$ angle. The heel accelerometer makes, on average, a positive 6.8° angle with the reference axis. When we subtract these two averages, we get an angle of 13.6°. This is the angle of pronation that was discussed in the **Background** section. According to our cutoff ranges, Subject 1 is past 10°, so they would be pronating by about 3.6°. While this suggests that Subject 1 does pronate in a neutral stance, some errors must first be considered.

During the field tests, the accelerometers were not aligned to a known horizontal, they were just placed to our visual satisfaction of being parallel with the ground. What this means is that there could be an offset to the data by a few degrees. Had this offset been recorded during the data collection stages, we could have subtracted it from the data. Since the offset is unknown, we can only assume what it may have been. We do know that the offset should be within around 10°, because anything greater would have been noticeable to us when installing the accelerometers on the subject. A reasonable offset that we could infer would be a positive 4°. Subtracting this from our 13.6° result would leave us with an angle of 9.6°. This would mean that Subject 1 does not pronate past 10°, which falls in line with Subject 1 not having a history of pronation. While we established this baseline, it is not fully indicative of pronation or supination during motion like walking or running. The static cases were compared to the dynamic motion cases that followed.

In the dynamic case, PR and SP are most important to be measured when in the contact phase of the stride. Each stride is broken up by purple lines on the graphs. The contact phase can be identified by looking at when the FSRs are recording a force. So, in the slow walk and running data graphs, the FSRs are only active for about half a stride length. This half-stride length is what we will focus on when determining PR and SP. This also alleviates some of the concerns about the angles growing far past the standing values of those angles. When they do grow to the more extreme values, it is when the leg is moving laterally through the air, and, as mentioned above, lateral acceleration introduces error into the calculation of roll and pitch. The lateral acceleration induces acceleration values in the $x$ and $y$-axes of the accelerometer, changing the component values of Earth's gravity, which would in turn change the derived angle between the coordinate systems. Even with the complementary filter active, an excessive lateral motion will cause sizable spikes, like in our running graphs. A way of alleviating this further would be to use the Kalman filter discussed previously.

With this in mind, the observed average values from the walking plots are as follows. The lower calf has an average angle of $-6°$ and the heel has an average angle of 6° when looking at the mid point of the stride as indicated by the FSR readings. Taking the difference of them would result in an angle of 12°. This would go past our 10° cutoff but after subtracting out the implied offset of 4° the angle would be 9° which is within a normal range. This makes sense with our standing data result of 9.6° as it is not possible for the person to move too far away from the neutral position.

Moving on to the jogging plots, they are a bit more sporadic than the walking plots, but this is to be expected as the accelerometers are reading larger acceleration values which introduce more noise. The same analysis for standing and walking does not yield consistent results because the angles at the midpoints of the stride vary too much. A visual representation of the above discussion is shown in the plots below.

For each of the two figures below, the top graph displays the times during which the subject is pronating for the jogging data. The green line represents the pronation cutoff determined by Genova and Gross. Any point above this line is defined as a point in which the subject is pronating. The bottom graph displays the same information for supinating; however, the time when the subject supinates is defined as the points below the green cutoff.

We had both of our subjects attempt to intentionally pronate or supinate while standing, and while in motion. Data from these trials did not show any distinguishable difference compared to the normal trials. This could be a point of future research with a more more precise sensor and experimental setup.

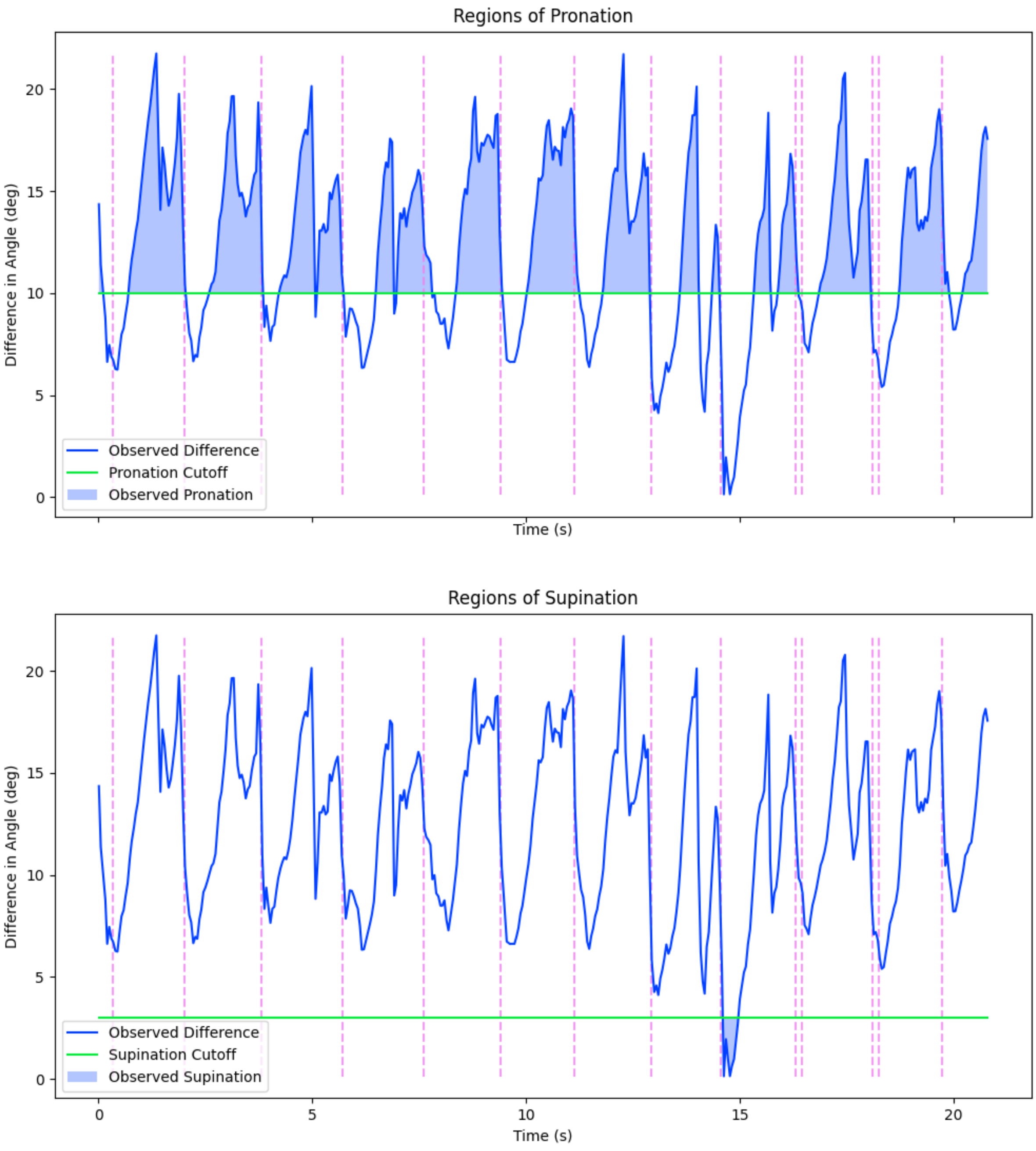

Figure 5.1: Pronation and supination while walking

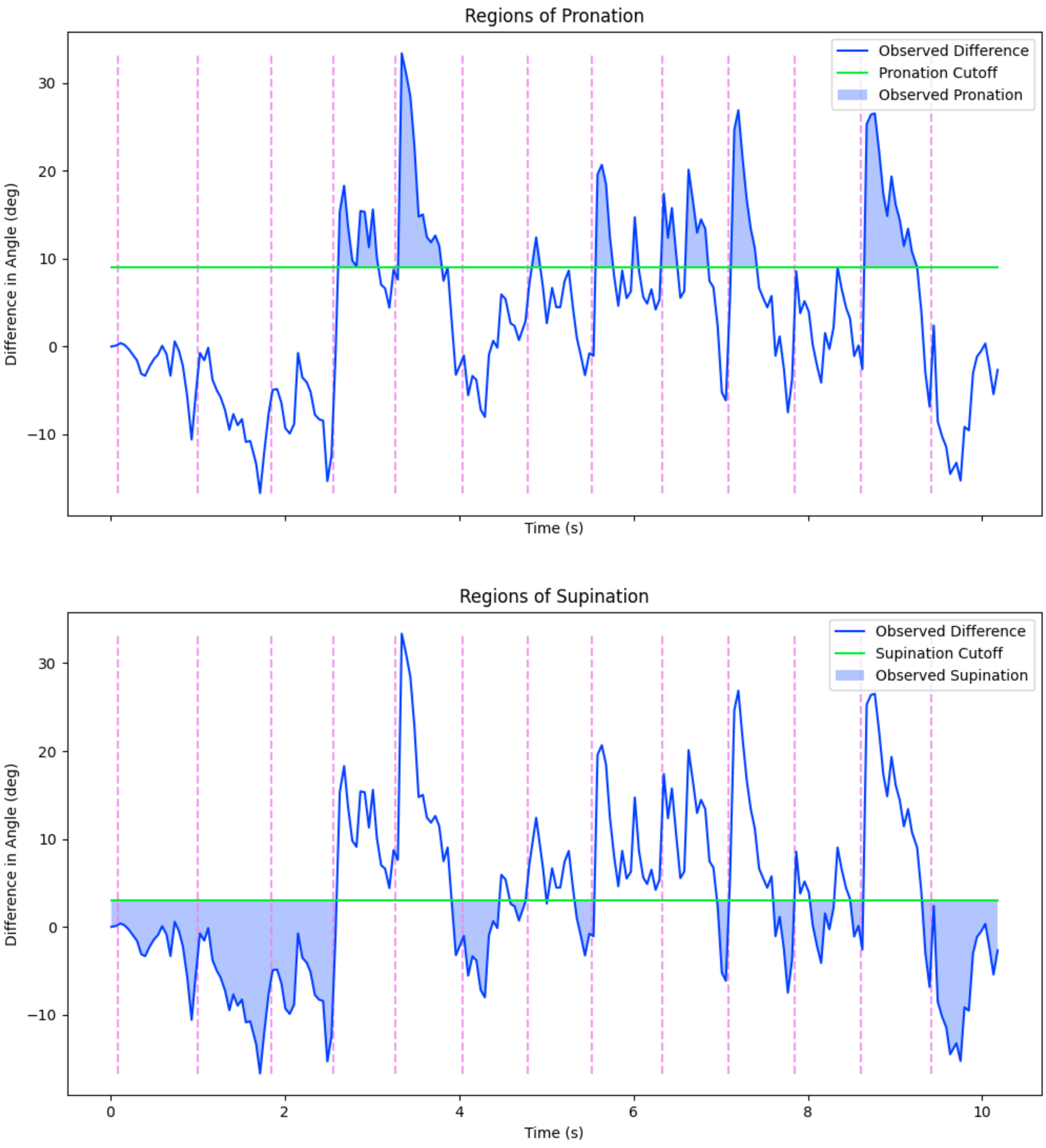

Figure 5.2: Pronation and supination while jogging

# Conclusion

Using a combination of force data collected using force sensitive resistors (FSRs) and angular displacement data collected using accelerometers, we were able to suggest how a person's foot might pronate or supinate during dynamic motion. None of our subjects showed any strongs signs of overpronation from the data. Even in the cases where we had the subject purposely pronate and supinate, the effect was minimal. While the sample size of this experiment is small, the creation of a low-cost device to measure pronation and supination could prove useful in further studies with larger sample sizes, especially if subjects who have a known medical history of pronation or supination could be gathered.

# Acknowledgements

We would like to thank Professor George Gollin and Ivan Velkovsky for their guidance and the Physics Department of the University of Illinois at Urbana-Champaign for providing the materials to create our project.

# List of Figures

# References

Adafruit Industries. (2021). *Adafruit triple-axis accelerometer - ±2/4/8g @ 14-bit - MMA8451*. Adafruit Industries. Retrieved April 16, 2021, from https://www.adafruit.com/product/2019

Erickson, V., Kamthe, A., & Cerpa, A. (2009). Demo abstract: Measuring foot pronation using rfid sensor networks. *SenSys '09: Proceedings of the Seventh ACM Conference on Embedded Network Sensor Systems*. https://doi.org/https://doi.org/10.1145/1644038.1644083

Genova, J. M., & Gross, M. T. (2000). Effect of foot orthotics on calcaneal eversion during standing and treadmill walking for subjects with abnormal pronation [PMID: 11104377]. *Journal of Orthopaedic & Sports Physical Therapy*, *30*(11), 664–675. https://doi.org/10.2519/jospt.2000.30.11.664

Grahn, E. (2017). *Evaluation of MEMS accelerometer and gyroscope for orientation tracking nutrunner functionality* (Bachelor's Thesis). KTH Royal Institute of Technology. https://www.diva-portal.org/smash/get/diva2:1146723/FULLTEXT01.pdf

Griffiths, I. (2021). *What is overpronation?* Kinetic Revolution. Retrieved April 16, 2021, from https://www.kinetic-revolution.com/overpronation-accurate-or-out-of-date-terminology

Menz, H. B., Dufour, A. B., Riskowski, J. L., Hillstrom, H. J., & Hannan, M. T. (2013). Association of planus foot posture and pronated foot function with foot pain: The framingham foot study. *Arthritis Care & Research*, *65*(12), 1991–1999. https://doi.org/https://doi.org/10.1002/acr.22079

Neumann, D. A. (2017). *Kinesiology of the muscoloskeletel system: Foundations for rehabilitation* (3rd ed.). Elsevier.

Newton, A. (2020, September 17). *Measure tilt angle using MPU6050 gyro/accelerometer & Arduino*. How To Electronics. https://how2electronics.com/measure-tilt-angle-mpu6050-arduino

Pedley, M. (2013, March). *Tilt sensing using a three-axis accelerometer*. Version 6. NXP Semiconductors. https://www.nxp.com/docs/en/application-note/AN3461.pdf

Python Software Foundation. (2004, August 22). *The zen of Python*. Python Software Foundation. Retrieved April 19, 2021, from https://www.python.org/dev/peps/pep-0020

Richards, C. E., Magin, P. J., & Callister, R. (2009). Is your prescription of distance running shoes evidence-based? [Abstract]. *British Journal of Sports Medicine*, *43*(3), 159–162. https://doi.org/10.1136/bjsm.2008.046680

Tekscan. (2021a). *The gait cycle: Phases, parameters to evaluate & technology*. Tekscan. Retrieved April 16, 2021, from https://www.tekscan.com/print/blog/medical/gait-cycle-phases-parameters-evaluate-technology

Tekscan. (2021b). *How to convert resistance (Ohms) to force (lbs)?* Tekscan. Retrieved April 16, 2021, from https://www.tekscan.com/support/faqs/how-convert-resistance-ohms-force-lbs

Tekscan. (2021c). *Small force sensing resistor*. Tekscan. Retrieved April 16, 2021, from https://www.tekscan.com/products-solutions/force-sensors/a201

Tsai, L.-C., Yu, B., Mercer, V. S., & Gross, M. T. (2006). Comparison of different structural foot types for measures of standing postural control [PMID: 17193872]. *Journal of Orthopaedic & Sports Physical Therapy*, *36*(12), 942–953. https://doi.org/10.2519/jospt.2006.2336

Willems, T. M., Ley, C., Goetghebeur, E., Theisen, D., & Malisoux, L. (2021). Motion-control shoes reduce the risk of pronation-related pathologies in recreational runners: A secondary analysis of a randomized controlled trial [PMID: 33306927]. *Journal of Orthopaedic & Sports Physical Therapy*, *51*(3), 135–143. https://doi.org/10.2519/jospt.2021.9710